Direct visualization of vortex pattern transition in ZrB$_{12}$ with Ginzburg-Landau parameter close to the dual point

Jun-Yi Ge,[1,*] Joffre Gutierrez,[1] A. Lyashchenko,[2] V. Filipov,[2] Jun Li,[1] and Victor V. Moshchalkov[1,†]

[1]*INPAC–Institute for Nanoscale Physics and Chemistry, KU Leuven, Celestijnenlaan 200D, B-3001 Leuven, Belgium*

[2]*Frantsevich Institute for Problems of Materials Science, NASU, 03680 Kiev, Ukraine*

In nature, many systems exhibit modulated phases with periodic macroscopic patterns and textures mainly due to the competitive interactions of different phases. Vortex systems in superconductors, which are easy to access, offer the possibility of tuning the ratio between the competitive interactions, providing a unique tool to study the evolution and equilibrium of similar patterns. The κ-T phase diagram of clean superconductors shows the transition from type-I to type-II superconductivity via a narrow κ range near the dual point $\kappa = 1/\sqrt{2}$ where the vortices attract each other at long distances and repel each other at short distances. This κ range, which is termed the type-II/1 phase, becomes larger with decreasing temperature. The direct imaging at the scale of individual vortices of the vortex pattern transition would provide valuable information. Therefore, by using scanning Hall probe microscopy, we have performed direct visualization of the vortex pattern transition in a ZrB$_{12}$ single crystal across the type-II and type-II/1 phases. By gradually lowering the temperature, and thereby tuning vortex interactions, a transition is observed from the ordered Abrikosov vortex lattice to a disordered vortex pattern with large areas of Meissner phase, vortex chains, and vortex clusters. The formation of vortex chains and clusters has been found to arise from the combined effect of quenched disorder and the attractive vortex-vortex interaction in the type-II/1 phase. The clusters and chains serve as the vortex reservoir to enable the formation of a triangular vortex lattice of the type-II phase at high temperatures.

I. INTRODUCTION

The morphology as well as the physical properties of different condensed matter systems are mainly defined by the interactions among relevant "elements." These interactions can either be monotonous (i.e., fully repulsive or attractive) or competing [1–6]. In physics, superconductivity offers a unique scenario to study different kind of interactions including vortex-vortex interactions. Due to its easy accessibility, one can tune various relevant parameters such as flux density B and interaction strength T or even control the amount of quenched disorder present in the system. On top of this, different superconducting systems present different types of the vortex-vortex interactions.

Commonly, superconductors are divided into two categories by using the Ginzburg-Landau (GL) parameter $\kappa = \lambda/\xi$ (λ is the penetration depth, ξ is the coherence length): type I with $\kappa < 1/\sqrt{2}$; type II with $\kappa > 1/\sqrt{2}$. These two kinds of superconductors display different orders of phase transition when approaching the normal state under the presence of a magnetic field, with a first-order transition for type I and second order for type-II superconductors. However, it is revealed that the superconducting to normal phase transition can be of both first and second order in superconductors with κ very close to the dual point $1/\sqrt{2}$, which was coined as type-II/1 phase by Auer and Ullmaier [7] in order to distinguish it from the Shubnikov phase in traditional type-II superconductors (type-II/2). The phase transitions can be differentiated by the isothermal magnetization measurements, where the type-II/1 superconductors experience a first-order transition at H_{c1} with

a magnetization jump and then progressively transit to the normal state at H_{c2} like the normal type-II/2 superconductors [Fig. 1(e)]. The κ-t ($t = T/T_c$) phase diagram has also been made through the study of several low-κ superconductors [7,8], as shown in Fig. 1(a).

In type-II/2 superconductors, vortex-vortex interaction is purely repulsive; due to that, the most energetically favorable state is the triangular ordered vortex lattice (VL), which is well known as the Abrikosov VL [e.g., the lower panel of Fig. 1(b) for NbSe$_2$]. On the contrary, in type-I superconductors with a finite demagnetization factor N, the interaction between vortices becomes long-range repulsive and short-range attractive. Flux units tend to merge with each other to form flux tubes (giant vortices) and stripes (large normal domains) as shown in the upper panel of Fig. 1(b) for a type-I Pb film. Yet, in type-II/1 superconductors, vortices penetrate in at $H_p = (1 - N)H_{c1}$ and form the intermediate mixed state (IMS) with domains of triangular VL surrounded by large areas of the Meissner state [9]. The IMS is explained by the competition of long-range attractive and short-range repulsive interactions among vortices [10].

The phase diagram of low-κ clean superconductors in the κ-t plane was first computed from BCS-Gor'kov-Eilenberger theory by Klein [11]. Nevertheless, so far, the phase transitions and related vortex patterns for type-II/1 superconductors are not well understood, mainly because of the lack of low-κ superconductors, the interplay of quenched disorder, and the proper technique to visualize the vortices. Ever since the early reports of the IMS observed by the Bitter decoration technique about 40 years ago [12,13], most work has been focused on theoretical simulations, and various vortex patterns have been predicted [10,14–19]. By using the small-angle neutron scattering technique, the morphology of the vortex pattern in low-κ Nb superconductors has been reported [20–22]. So far,

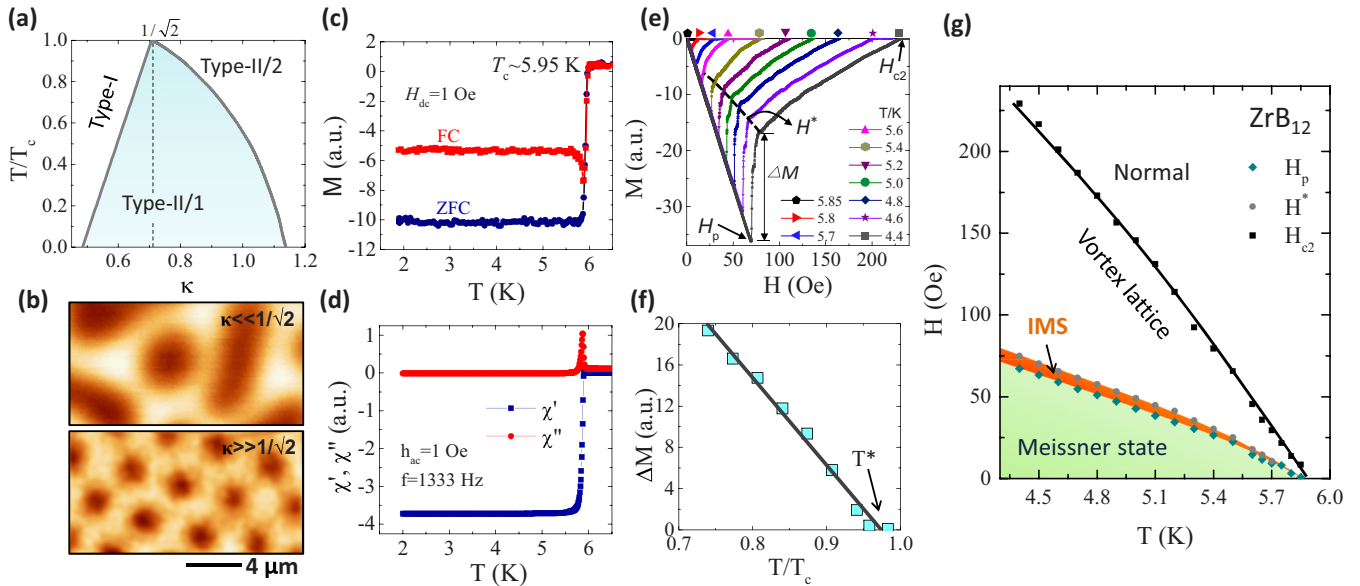*junyi.ge@fys.kuleuven.be

†victor.moshchalkov@fys.kuleuven.be

FIG. 1. (Color online) Sample characterization and vortex phase diagram. (a) Representation of the κ-t phase diagram. The shaded area represents the type-II/1 regime close to the dual point. (b) Typical images of the vortex patterns for the well-known type-I superconductor Pb (upper) and type-II/2 superconductor NbSe$_2$ (lower). The dark (bright) area represents the normal (superconducting) state. (c) Zero-field-cooling (ZFC) and field-cooling (FC) measurements of dc magnetization in a field of 1 Oe. The difference between FC and ZFC curves at low temperatures indicates the presence of pinning in the material. (d) In-phase and out-of-phase ac susceptibility measured at $h_{ac} = 1$ Oe, $f = 1333$ Hz. (e) Virgin M-H curves for ZrB$_{12}$ at various temperatures. The dashed line marks the position of H^*, above which type-II behavior dominates. (f) The magnetization jump at H_p as a function of reduced temperature. By extrapolating the linear dependence, ΔM disappears at $T^* \sim 0.97 T_c$. (g) H-T phase diagram showing different regimes of vortex phases, where the type-II/1 regime only occupies a narrow area.

no local direct observation has been provided, especially in superconductors with quenched disorder, where the use of the neutron scattering technique is quite limited.

In this article, we report the vortex evolution from the type-II/1 to the type-II/2 phase in a low-κ superconductor ZrB$_{12}$ single crystal by varying the temperature. Close to T_c in the type-II/2 phase, an Abrikosov VL is well formed. On decreasing temperature the VL undergoes a transition toward a square VL. By further decreasing the temperature the system transits to the type-II/1 phase, where very inhomogeneous vortex patterns have been observed with vortex chains, vortex clusters, and isolated vortices surrounded by large Meissner areas. The formation of the vortex clusters is studied in detail, and the important contribution of the quenched disorder is revealed.

II. EXPERIMENTAL

The study is performed on a high-quality single crystal of ZrB$_{12}$ with $T_c \sim 5.95$ K as deduced from the dc and ac magnetization measurements [Figs. 1(c) and 1(d)]. The ZrB$_{12}$ single crystal was prepared by the inductive zone melting method [23]. The crystal has a very flat surface with a roughness around 2 nm, as shown in Fig. s1 of the Supplemental Material [24]. Bulk magnetization measurements were carried out with a SQUID from Quantum Design. Local magnetic field measurements were carried out by using a modified scanning Hall probe microscope (SHPM) from Nanomagnetics Instruments with a temperature stability better than 1 mK and a magnetic field resolution of 0.1 Oe. The images were recorded in lift-off mode by moving the Hall cross above the sample surface at a height of about 1 μm.

All the experiments were performed with the field applied perpendicular to the sample surface.

III. RESULTS AND DISCUSSIONS

A. Vortex phase diagram

Figure 1(e) presents the virgin $M(H)$ curves at various temperatures. It is clear that below the penetration field H_p the sample is in the Meissner state. At H_p the $M(H)$ curves exhibit an abrupt magnetization jump ΔM due to the attractive vortex interaction, and the magnetic field penetrates in the sample to form the IMS. When the magnetic field reaches H^*, another discontinuity appears, then M gradually decreases to 0 at H_{c2}. With increasing temperature, the magnetization jump ΔM is suppressed and traditional type-II behavior dominates [25]. This can better be seen in Fig. 1(f) where ΔM follows a linear dependence with temperature as indicated by the solid line, and above $T^* \sim 0.97 T_c$, ΔM decreases to zero, indicating the repulsive interaction prevails. The observed behavior is very similar to another type-II/1 superconductor Nb reported before [8]. Since ZrB$_{12}$ has a GL parameter κ very close to the $1/\sqrt{2}$, small changes in the sample preparation process (e.g., defect concentration and thermal treatment) could result in the change of G-L parameter. The preparation method used for our crystal yields typically a κ value between 0.8 and 1.12. The phase diagram deduced from above is shown in Fig. 1(g). Three magnetic phases are observed, with the IMS only occupying a narrow area on the phase diagram. However, it should be noted that due to the existence of a surface barrier and random pinning produced by the quenched disorder, the
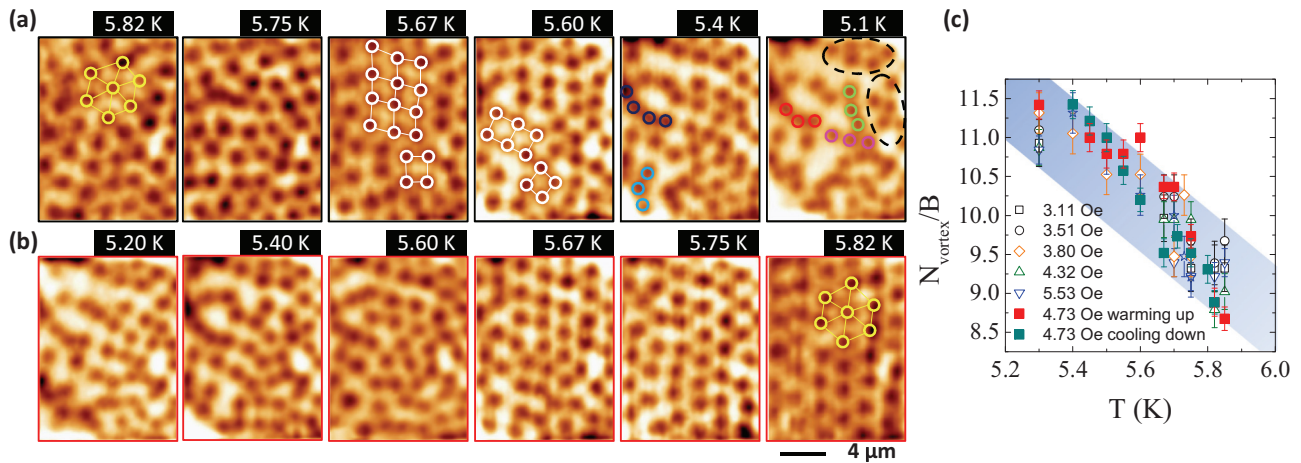
FIG. 2. (Color online) Vortex pattern evolution with cycling temperature after FC using $H = 4.73$ Oe. (a) SHPM images observed with decreasing temperature. The dark spots represent vortices. A distorted triangular VL is observed at 5.82 K as highlighted by the symbols. With decreasing temperature, vortices tend to form a square lattice, as indicated by the white squares, and then transform to a disordered state with vortex chains (open symbols) and clusters (dashed circle) as can be seen at 5.4 and 5.1 K. (b) When cycling the temperature back, a disorder-to-order transition of the vortex arrangement is recovered. (c) The normalized number of vortices observed in the scanned area as a function of temperature under various fields. The increasing trend with decreasing temperature suggests that the vortex pattern is compressed by the vortex attraction in the scanned area, resulting in areas of the sample free of vortices.

vortex patterns nucleated above H_{c1} can still be observed even when entering in the Meissner state by, for example, performing a field-cooling (FC) process.

B. Vortex pattern evolution

To study the vortex patterns in the different phases mentioned above, we perform FC first and then map the field distribution while progressively cycling the temperature. Images are taken under isothermal conditions. The evolution of the vortex patterns for a FC under a magnetic field of 4.73 Oe is shown in Fig. 2. The dark spots represent vortices, while the intervortex superconducting states are displayed as bright areas. At 5.82 K the Abrikosov VL is well formed indicating the sample is in the traditional type-II/2 regime. Note that the triangular VL is distorted, due to the existence of quenched disorder. In some other areas with fewer defects, a well-ordered triangular lattice is formed at high temperatures (see Fig. s3 of the Supplemental Material [24]). With decreasing temperature, the VL becomes more and more disordered as a result of the increase of the attractive interactions among vortices. At intermediate temperatures, a square lattice is energetically favorable as shown by the white circles at 5.67 and 5.6 K (also see Fig. s4 in the Supplemental Material). The change from triangular lattice to square lattice is also confirmed by the Fourier transform of corresponding images (see Supplemental Material, Fig. s5). A square lattice has also been suggested for another low-κ material (Nb) from the neutron diffraction measurements [20]. Very recently, Meng *et al.* [26] proposed that the various vortex symmetries, including the square lattice, can be generated in superconducting systems with multiscale intervortex interactions, which is in accordance with our findings. At still low temperatures, vortices finally form vortex chains and clusters, as indicated by the open symbols and dashed circles, respectively. This order-disorder transition can be reversed by warming up the sample across the phase

boundaries as presented in Fig. 2(b). We have repeated the whole process at several randomly chosen locations. All of them show similar phenomena as discussed above.

The observation of vortex chains is quite interesting. A similar phenomenon has been observed in many physical systems with competitive interactions. For example, in the transition from the vortex solid to vortex liquid phase, the thermal fluctuations overcome the vortex repulsive interaction and linear vortex arrangement appears [27]. Here, the competition arises from the short-range repulsive and long-range attractive interactions. A close resemblance has also been found compared to the vortex patterns in the type-1.5 superconductor MgB_2, where vortex stripes and clusters are formed under the competition of long-range attraction and short-range repulsion among vortices due to the two-band effect [28–31]. We have also counted the number of vortices in each image as displayed in Fig. 2(c). It is seen that with decreasing temperature, the number of vortices in the scanned area increases. This suggests that the vortex pattern is compressed, which provides evidence of the long-range attractive interaction. As a consequence, in some other areas, there are fewer vortices compared to the current location, which will be shown below (Figs. 3 and 4).

We also notice that in some scanned areas, there exists a hysteresis from the disorder-to-order transition when warming up the sample. Only at higher temperatures can the vortex pattern recover the same ordered state as the one obtained during the initial FC. This might be related to the presence of random pinning in the material. When performing field cooling from high temperature, the vortices nucleated in the sample are homogeneously distributed. The main interaction among vortices is repulsive, leading to the formation of the Abrikosov VL. With decreasing temperature an attractive interaction between vortices starts to develop, leading to vortex accumulation in order to balance the resulting increase in energy. The presence of quenched disorder in the sample gives rise
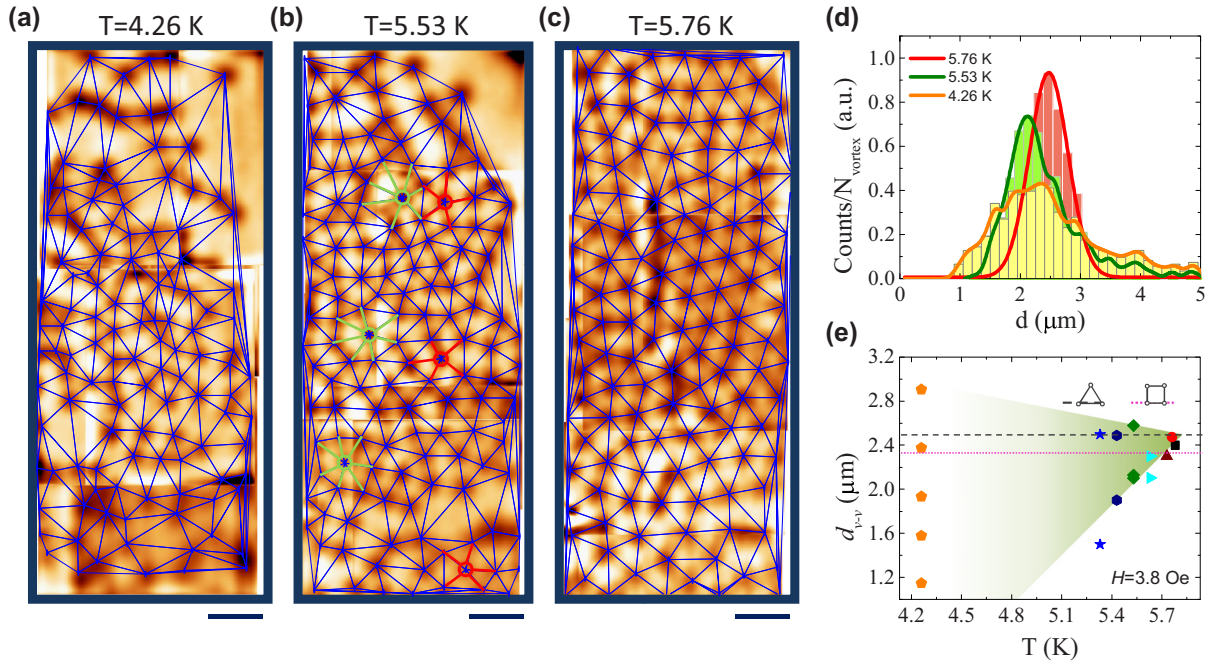
FIG. 3. (Color online) Vortex pattern nucleated after FC to various temperatures at $H = 3.8$ Oe. The Delaunay triangulation of the vortex pattern is also shown in each panel, where the vertices of each triangle represent the locations of the vortices. The scale bar below each image represents 4 μm. (a) At $T = 4.26$ K, a very inhomogeneous pattern is observed with vortices accumulated in the central part of the scanned area. (b) When increasing temperature to 5.53 K, vortices begin to expand due to the decrease of the attractive interaction, and seven-fold- and five-fold-coordinated vortices can be observed, as highlighted by the green and red lines, respectively. (c) At 5.76 K, vortices are distributed homogeneously in the whole pattern with most of them having six-fold coordination. (d) Histogram of the nearest-neighbor distances for the vortex patterns at various temperatures. The bin size used here is 0.15 μm. The red line is a Gaussian fit to the histogram. The green and yellow lines are B-spline lines. At low temperatures, more distribution peaks appear. (e) Nearest-neighbor distance at the peak position as a function of temperature. The shaded area indicates the peak distribution width, which increases with decreasing temperature. The dashed and dotted lines correspond to the nearest-neighbor distance for a triangular and square lattice, respectively.

to a weak pinning landscape in ZrB$_{12}$, and as a consequence preferential positions exist for vortex nucleation, and vortices will cluster around them. When cycling the temperature back, vortices need a stronger repulsive force to overcome the pinning force. Therefore, the VL can only recover at higher temperature. Similar hysteresis effect has also been observed in the intermediate state of type-1 superconductors [32,33].

C. Statistics of vortex arrangement

To confirm the above hypothesis, we have stitched together a few SHPM images to visualize a larger sample area in both type-II/2 and type-II/1 regimes, as presented in Fig. 3. To show the vortex distributions more clearly, we plot the vortex positions for the ordered and disordered vortex patterns using the Delaunay triangulation method. At $T = 4.26$ K
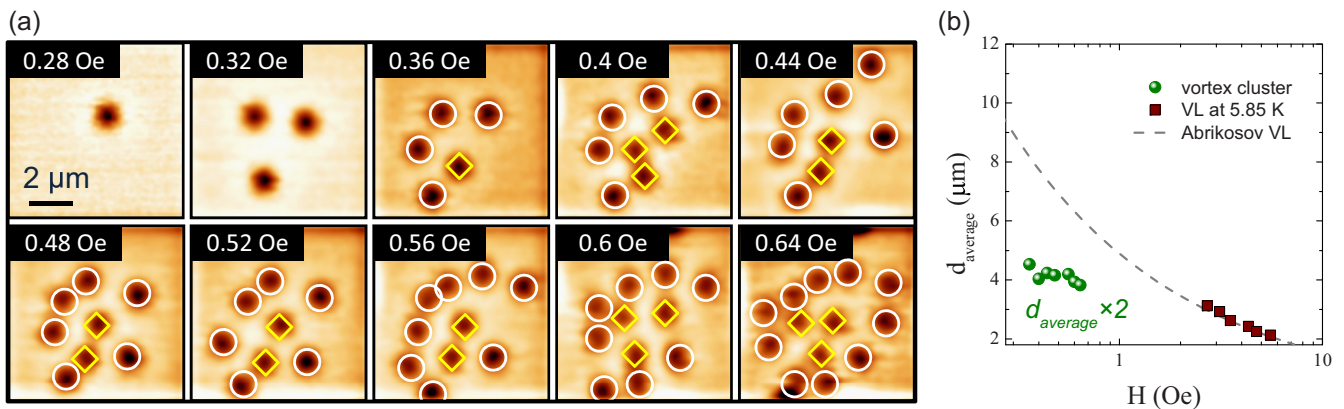

FIG. 4. (Color online) Vortex cluster formation. (a) SHPM images observed at 4.2 K after FC with progressively increasing magnetic fields, showing the formation of a vortex cluster. The symbols indicate the location of the vortices. (b) Averaged nearest-neighbor distance as a function of the applied magnetic field for the vortex cluster of (a). The nearest-neighbor distance for the VL at 5.85 K is shown by the squares, which well follows the triangular arrangement of the Abrikosov VL (dashed line).

[Fig. 3(a)], deep in the type-II/1 regime, a very inhomogeneous vortex pattern with vortex chains, clusters, and large Meissner (vortex-free) areas is observed. At $T = 5.53$ K [Fig. 3(b)], the highly dense vortex area expands due to the weakening of the attractive force with increasing temperature, resulting in a more ordered pattern. Seven-fold- and five-fold-coordinated vortices are observed in this temperature regime as highlighted by the green and red lines, respectively. At 5.76 K, the vortex pattern further expands with vortices distributed over the whole scanned area, forming an Abrikosov lattice. Most of the vortices have six-fold coordination. Notice that the Abrikosov lattice contains some defects as expected at low fields as a consequence of the presence of weak pinning [34].

The distribution of the first-neighbor distances d_{v-v} calculated for both ordered and disordered states is plotted in Fig. 3(d). The vortex distribution for the ordered state (squares) can be fitted by a Gaussian form with the maximum point of the statistics around 2.47 μm, which is consistent with the value ($\sim$ 2.5 μm) from the triangular VL at the same field using $d_{v-v}^2 = 2\phi_0/\sqrt{3}B$. In contrast, the disordered state shows a much broader distribution with additional peaks being observed. The observed vortex distribution peaks as a function of temperature are displayed in Fig. 3(e). It is seen that with decreasing temperature, the minimum d_{v-v} value at the peaks decreases while the peak distribution width (shown by the shaded area) increases. These results provide direct evidence for the attractive interactions between vortices at low temperatures.

The observed vortex distribution in the type-II/1 phase of ZrB$_{12}$ is remarkably different from those observed previously in other low-κ superconductors like in high-purity Nb samples [12,21,35], where the Meissner areas appear surrounded by mixed-state areas presenting a triangular VL. In our ZrB$_{12}$ single crystal, the vortex patterns in the type-II/1 phase are highly disordered, mainly composed of isolated vortices, and vortex clusters, and chains. It is clearly observed that the vortices that form the clusters are very close to each other. For example, some vortices inside the clusters shown in Fig. 3(e) have a first-neighbor separation of 1.15 μm. We also notice that the vortex clusters have very irregular shapes, which can be explained by the symmetry-breaking effect due to the presence of random pinning centers. Such a scenario is in good agreement with the theoretical simulations of a superconducting system with competing interactions and weak pinning centers [14,17]. We would like to stress that these disordered structures, appearing in the type-II/1 phase, have been observed all over the sample (see also in Supplementary Material V). We suggest that the vortex clusters play a role as the vortex reservoir in the type-II/1 phase. With increasing temperature, the vortex cluster will gradually expel the vortices to fill up the Meissner area and form the Abrikosov lattice of the type-II/2 phase.

D. Vortex cluster formation

To further understand how the vortices are distributed inside the vortex clusters, we have performed FC at various magnetic fields with 0.04-Oe dc field increment. The results are presented in Fig. 4(a). The vortices are shown by using different symbols:

(1) Core vortices, shown by diamonds, are the vortices located close to the pinning centers. After each field cooling, they always prefer to sit around the same locations. These vortices form the cluster cores.

(2) Fringe vortices, marked by open circles, nucleate around the core vortices at high temperatures and subsequently are pushed to them by the attractive interaction when cooling down to the type-II/1 regime.

Fringe vortices tend to form the triangular arrangement with core vortices, forming the periphery of the clusters. In this scenario, the vortex clusters can still be regarded as a distorted triangular VL. Notice, however, that the averaged first-neighbor distance inside the cluster exhibits a very weak dependence on the external field [Fig. 4(b)]. This is different from the case of clean low-κ superconductors, where Meissner areas appear surrounded by mixed-state areas presenting a triangular VL with constant vortex-vortex separation. The presence of weak pinning might lead to an inhomogeneous distribution of the attractive force, which needs further study. Additionally, it should be noted that no giant vortices are formed in the vortex cluster, suggesting the repulsive force dominates at short distances and the measured temperature range.

IV. CONCLUSION

In summary, we have presented the direct visualization, with single vortex resolution, of the vortex pattern transition in the low-κ ZrB$_{12}$ superconductor across its type-II/2 and type-II/1 phases. A wealth of previously unknown information has been obtained. In the type-II/2 phase, we have observed that weak pinning arising from the quenched disorder present in the sample creates only a small amount of defects in the Abrikosov lattice, as is predicted by the theory. In contrast, in the type-II/1 phase, the deviation from the vortex patterns observed in clean systems and from those predicted by simulations, which include random pinning, is much bigger. We observe a highly disordered state composed of a rich variety of structures, including vortex clusters, chains, and isolated vortices. That could be explained by the presence of long-range vortex attractions combined with randomly distributed pinning centers. We have also studied the evolution of the vortex clusters as we change the particle density and we have observed that clusters tend to form around energetically favored positions all over the sample. The vortices in the clusters arrange in a much distorted triangular symmetry, keeping their first-neighbor distances constant as the particle density is increased. The results presented here unveil the intricate process of phase transition in superconductors with competing interactions. Moreover, the detailed phase transition process also provides a reference as a general mechanism for other systems with similar particle interaction such as protein molecules in solutions.

[1] V. M. Kaganer, H. Mohwald, and P. Dutta, Rev. Mod. Phys. **71**, 779 (1999).

[2] M. Seul and D. Andelman, Science **267**, 476 (1995).

[3] N. Hoffmann, F. Ebert, C. N. Likos, H. Lowen, and G. Maret, Phys. Rev. Lett. **97**, 078301 (2006).

[4] A. I. Campbell, V. J. Anderson, J. S. van Duijneveldt, and P. Bartlett, Phys. Rev. Lett. **94**, 208301 (2005).

[5] F. F. Munarin, K. Nelissen, W. P. Ferreira, G. A. Farias, and F. M. Peeters, Phys. Rev. E **77**, 031608 (2008).

[6] G. R. Berdiyorov, A. D. Hernandez, and F. M. Peeters, Phys. Rev. Lett. **103**, 267002 (2009).

[7] J. Auer and H. Ullmaier, Phys. Rev. B **7**, 136 (1973).

[8] H. W. Weber, E. Seidl, M. Botlo, C. Laa, E. Mayerhofer, F. M. Sauerzopf, R. M. Schalk, and H. P. Wiesinger, Physica C **161**, 272 (1989).

[9] U. Krageloh, Phys. Lett. A **28**, 657 (1969).

[10] F. Mohamed, M. Troyer, G. Blatter, and I. Lukyanchuk, Phys. Rev. B **65**, 224504 (2002).

[11] U. Klein, J. Low Temp. Phys. **69**, 1 (1987).

[12] H. Trauble and U. Essmann, Phys. Stat. Sol. **20**, 95 (1967).

[13] U. Essmann and H. Trauble, Sci. Am. **224**, 75 (1971).

[14] H. J. Zhao, V. R. Misko, and F. M. Peeters, New J. Phys. **14**, 063032 (2012).

[15] J. A. Drocco, C. J. Olson Reichhardt, C. Reichhardt, A. R. Bishop, J. Phys: Condens. Matter **25**, 345703 (2013).

[16] P. Miranovic and K. Machida, Phys. Rev. B **67**, 092506 (2003).

[17] X. B. Xu, H. Fangohr, Z. H. Wang, M. Gu, S. L. Liu, D. Q. Shi, and S. X. Dou, Phys. Rev. B **84**, 014515 (2011).

[18] X. B. Xu, H. Fangohr, S. Y. Ding, F. Zhou, X. N. Xu, Z. H. Wang, M. Gu, D. Q. Shi, and S. X. Dou, Phys. Rev. B **83**, 014501 (2011).

[19] I. Luk'yanchuk, Phys. Rev. B **63**, 174504 (2001).

[20] S. Muhlbauer, C. Pfleiderer, P. Boni, M. Laver, E. M. Forgan, D. Fort, U. Keiderling, and G. Behr, Phys. Rev. Lett. **102**, 136408 (2009).

[21] M. Laver, C. J. Bowell, E. M. Forgan, A. B. Abrahamsen, D. Fort, C. D. Dewhurst, S. Muhlbauer, D. K. Christen, J. Kohlbrecher, R. Cubitt, and S. Ramos, Phys. Rev. B **79**, 014518 (2009).

[22] H. W. Weber, E. Seidl, M. Botlo, C. Laa, E. Mayerhofer, F. M. Sauerzopf, R. M. Schalk, H. P. Wiesinger, and J. Rammer, Physica C **161**, 272 (1989).

[23] D. Daghero, R. S. Gonnelli, G. A. Ummarino, A. Calzolari, Valeria Dellarocca, V. A. Stepanov, V. B. Filippov, and Y. B. Paderno, Supercond. Sci. Technol. **17**, S250 (2004).

[24] See Supplemental Material at http://link.aps.org/supplemental/10.1103/PhysRevB.90.184511 for vortices form well ordered triangular lattice at 5.8 K while at low temperatures (5.0 K), less vortices is observed since some of them are pushed to the area with relatively stronger pinning centers (as discussed in the main text) due to the vortex-vortex attraction.

[25] W. De Sorbo, Rev. Mod. Phys. **36**, 90 (1964).

[26] Q. Meng, C. N. Varney, H. Fongohr, and E. Babaev, Phys. Rev. B **90**, 020509(R) (2014).

[27] I. Guillanmon, H. Suderow, A. Fernandez-Pacheco, J. Sese, R. Cordoba, J. M. De Teresa, M. R. Ibarra, and S. Vieira, Nat. Phys. **5**, 651 (2009).

[28] V. V. Moshchalkov, M. Menghini, T. Nishio, Q. H. Chen, A. V. Silhanek, V. H. Dao, L. F. Chibotaru, N. D. Zhigadlo, and J. Karpinski, Phys. Rev. Lett. **102**, 117001 (2009).

[29] E. Babaev and M. Speight, Phys. Rev. B **72**, 180502(R) (2005).

[30] E. Babaev and N. W. Ashcroft, Nat. Phys. **3**, 530 (2007).

[31] J. Gutierrez, B. Raes, A. V. Silhanek, L. J. Li, N. D. Zhigadlo, J. Karpinski, J. Tempere, and V. V. Moshchalkov, Phys. Rev. B **85**, 094511 (2012).

[32] J. Ge, J. Gutierrez, B. Raes, J. Cuppens, and V. V. Moshchalkov, New J. Phys. **15**, 033013 (2013).

[33] J. Ge, J. Gutierrez, J. Cuppens, and V. V. Moshchalkov, Phys. Rev. B **88**, 174503 (2013).

[34] A. I. Larkin and Y. N. Ovchinnikov, J. Low Temp. Phys. **34**, 409 (1979).

[35] E. H. Brandt and M. P. Das, J. Supercond. Nov. Magn. **24**, 57 (2011).